



Supplement of

Non-steady-state stomatal conductance modeling and its implications: from leaf to ecosystem

Ke Liu et al.

Correspondence to: Ke Liu (klliu@caltech.edu) and Christian Frankenberg (cfranken@caltech.edu)

The copyright of individual parts of the supplement might differ from the article licence.

S1 Supplementary Information Text

S1.1 Climate Modeling Alliance (CliMA) Land Configuration

In this study, we mainly employed the soil-plant-air continuum (SPAC) module of CliMA Land (github.com/CliMA/Land) to run simulations with different stomatal modeling frameworks. The SPAC module consists of four key sub-modules: canopy radiative transfer (RT), plant hydraulics, photosynthesis, and stomatal models (Figure S1). At each time-step, the SPAC module first calls the canopy RT module to compute the radiation condition for each canopy layer and leaf angle group, then it uses the photosynthesis, plantHydraulics and stomatal models modules to calculate the leaf-level stomatal conductance and photosynthesis rates, based on which it computes the canopy fluxes (Wang et al., 2023).

For the canopy RT, we employed a vertically layered canopy scheme with leaf angular distribution and a hyperspectral radiation transfer scheme (adapted from the Soil Canopy Observation of Photosynthesis and Energy fluxes model (SCOPE); (van der Tol et al., 2009; Yang et al., 2017)). For the photosynthesis module, we used the classic photosynthesis model developed by Farquhar et al. (1980) for C3 plants. For the stomatal models, due to the limited availability of hydraulic traits data in the test region, we applied a tuning factor based on soil water potential rather than plant hydraulics to g_1 to account for the response of stomata to water supply. The boundary layer conductance to water (g_{bw}) of leaf level predictions were prescribed using the estimated g_{bw} provided in LI6800 measurements. The g_{bw} in canopy scale simulations was assumed to be a constant at $3 \text{ mol m}^{-2} \text{ s}^{-1}$, which is a relatively high conductance to make sure that the boundary layer conductance is not the main limiting factor of CO_2 supply (as our focus is on effects from stomatal conductance). We acknowledge more realistic g_{bw} values including calculation from wind speed and leaf width, which requires vertically resolved heterogeneous micro-climates and is under development.

In the steady-state mode, we ran iterations of the SPAC functions to find the stable solution for the given conditions at each time-step. In the prognostic mode, the simplified stomatal model was solved using the Euler method with a fixed step size, which is the time step used in each simulation. As current LSMs commonly use a time-step of 30 min or 60 min, we tested the stability of our model on 2, 6, and 10 min resolution for efficiency comparison, besides the fine 1 min resolution for flux comparison. We also tested that our method provides similar results with a much finer time step (1s, 1/60 of the 1min time step used for the comparison), the relative difference is minimal, $0.2 \pm 0.1 \%$, indicating the time step we chose is sufficient for our simulations and comparison.

Vegetation traits and properties, including leaf chlorophyll content, leaf mass per area, leaf photosynthetic capacity, stomatal model g_1 , Leaf area index, clumping index were prescribed for the test region, extracted from the global datasets (Croft et al., 2020; Butler et al., 2017; Luo et al., 2021; De Kauwe et al., 2015; Yuan et al., 2011; He et al., 2012). In this study, CliMA Land simulations were conducted offline. Environmental drivers (e.g. air temperature, dew-point temperature, volumetric soil water, wind speed etc.) were extracted from ERA5 reanalysis datasets (Hersbach et al., 2018) and updated accordingly at each step.

S2 Supplementary Figures

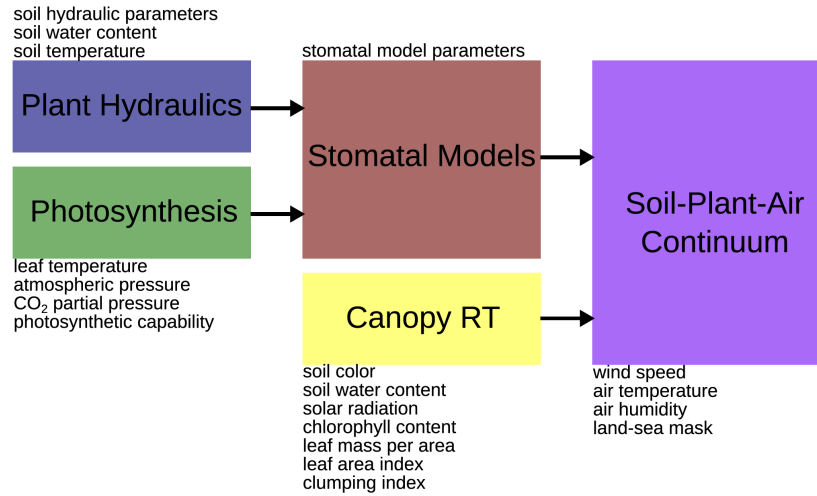


Figure S1: Model hierarchy of soil-plant-air continuum (SPAC) module of CliMA Land (from Wang et al. (2023)). Black arrows indicate the dependencies within the SPAC module, and the text next to each box describes the main parameters and weather drivers used in CliMA Land.

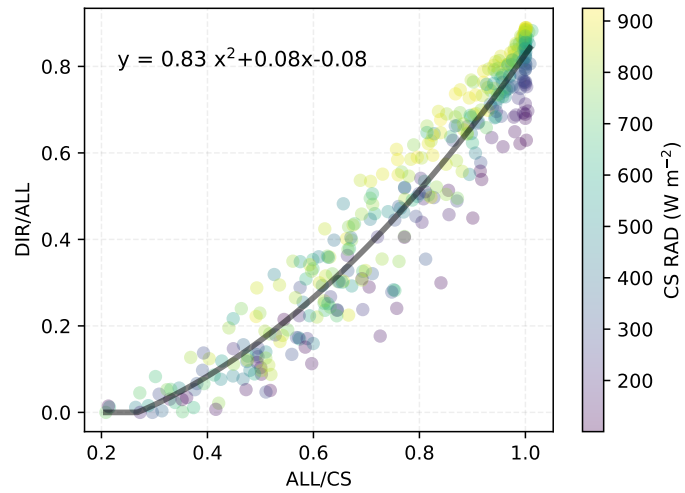


Figure S2: The empirical relationship between the direct radiation (DIR) fraction and the ratio between the total downward solar radiation (ALL) and the clear sky radiation (CS) in August 2017, filtered by 100 W m^{-2} CS radiation. Radiations are from the ERA5-Land hourly dataset.

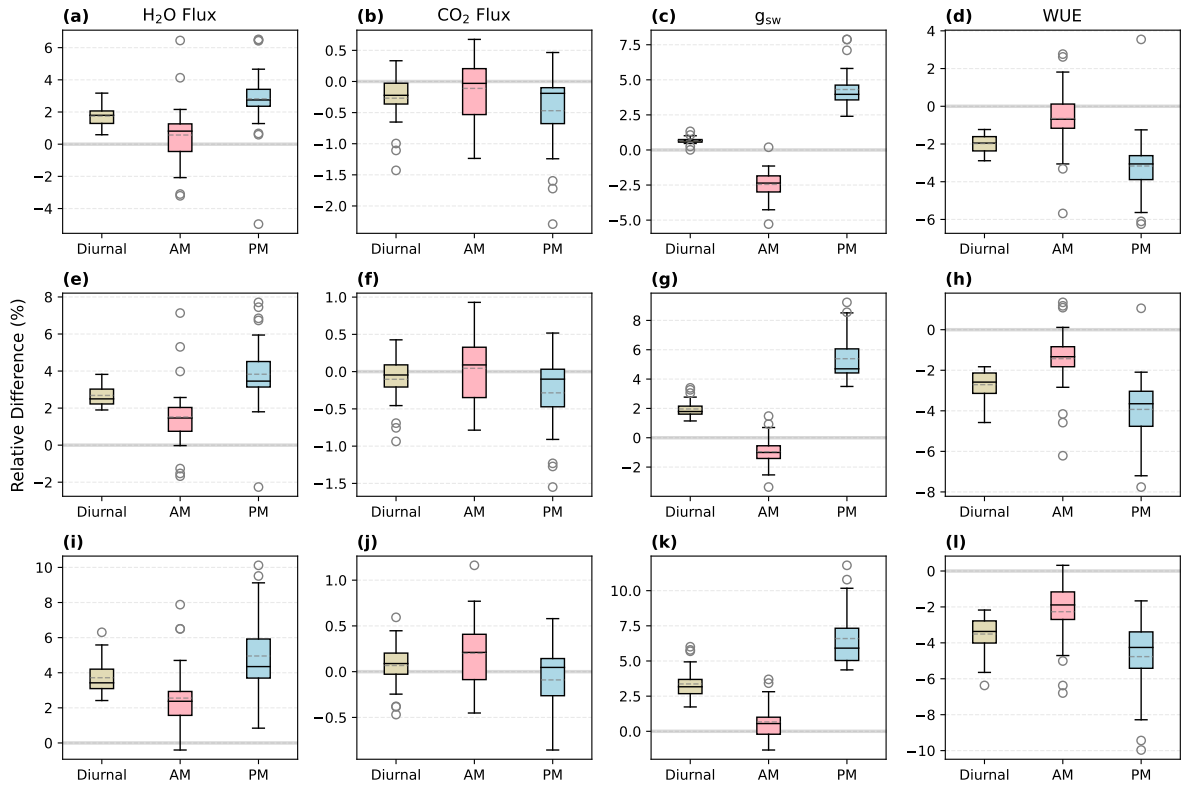


Figure S3: Relative differences (NSS - SS; RD) in the predicted daytime-mean fluxes of the NSS and SS simulations for August 2017, for results when $\tau_{op}/\tau_{cl} < 1$. The solid line in each box indicates the median, and the dashed line represents the mean. The results for the transpiration rate (H₂O flux), net productivity (CO₂ flux), canopy-averaged stomatal conductance to water (g_{sw}), and water-use efficiency (WUE) are shown in the respective columns from left to right. (a-d) $\tau_{op} = 750$ s, $\tau_{cl} = 900$ s, (e-h) $\tau_{op} = 600$ s, $\tau_{cl} = 900$ s, (i-l) $\tau_{op} = 450$ s, $\tau_{cl} = 900$ s. Diurnal: 5:00-19:00, AM: 5:00-12:00, PM: 12:00-19:00.

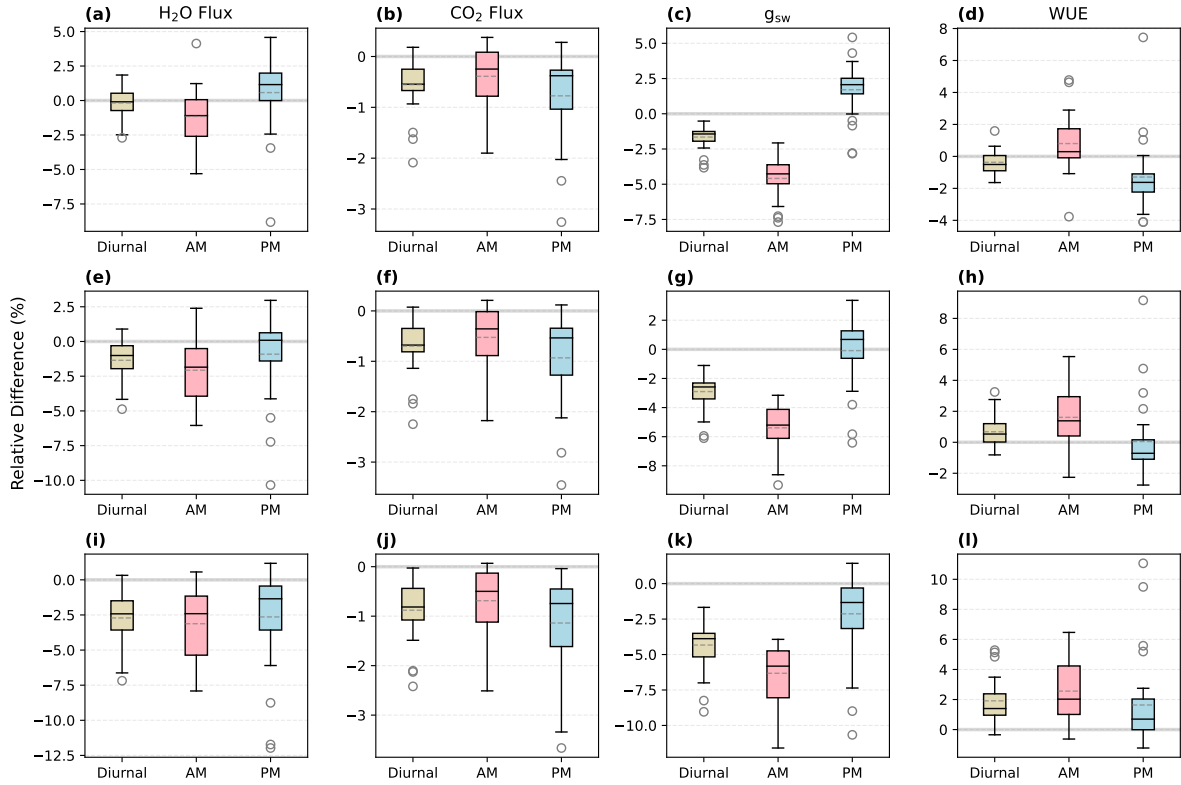


Figure S4: Relative differences (NSS - SS; RD) in the predicted daytime-mean fluxes of the NSS and SS simulations for August 2017, for results when $\tau_{op}/\tau_{cl} > 1$. The solid line in each box indicates the median, and the dashed line represents the mean. The results for the transpiration rate (H₂O flux), net productivity (CO₂ flux), canopy-averaged stomatal conductance to water (g_{sw}), and water-use efficiency (WUE) are shown in the respective columns from left to right. (a-d) $\tau_{op} = 900$ s, $\tau_{cl} = 750$ s, (e-h) $\tau_{op} = 900$ s, $\tau_{cl} = 600$ s, (i-l) $\tau_{op} = 900$ s, $\tau_{cl} = 450$ s. Diurnal: 5:00-19:00, AM: 5:00-12:00, PM: 12:00-19:00.

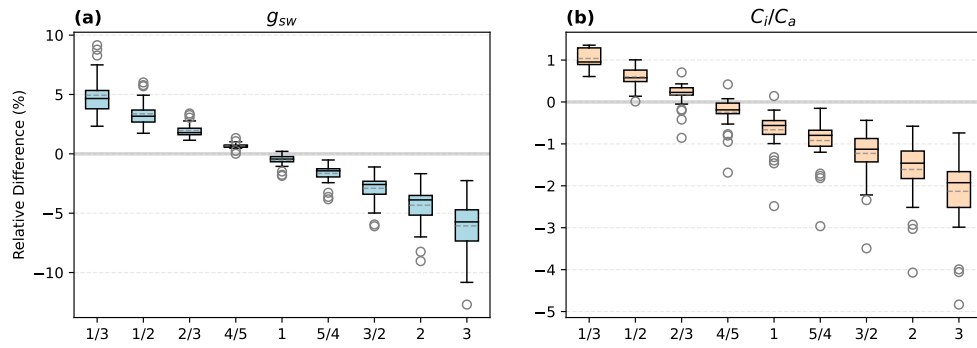


Figure S5: Relative differences (NSS - SS; RD) in the predicted daytime-mean (5:00-19:00) (a) canopy-averaged stomatal conductance to water (g_{sw}) and (b) intercellular CO_2 concentration (C_i). The solid line in each box indicates the median, and the dashed line represents the mean. Labels on the x-axis indicate the ratio between τ_{op} and τ_{cl} , with the larger one kept as 900 s

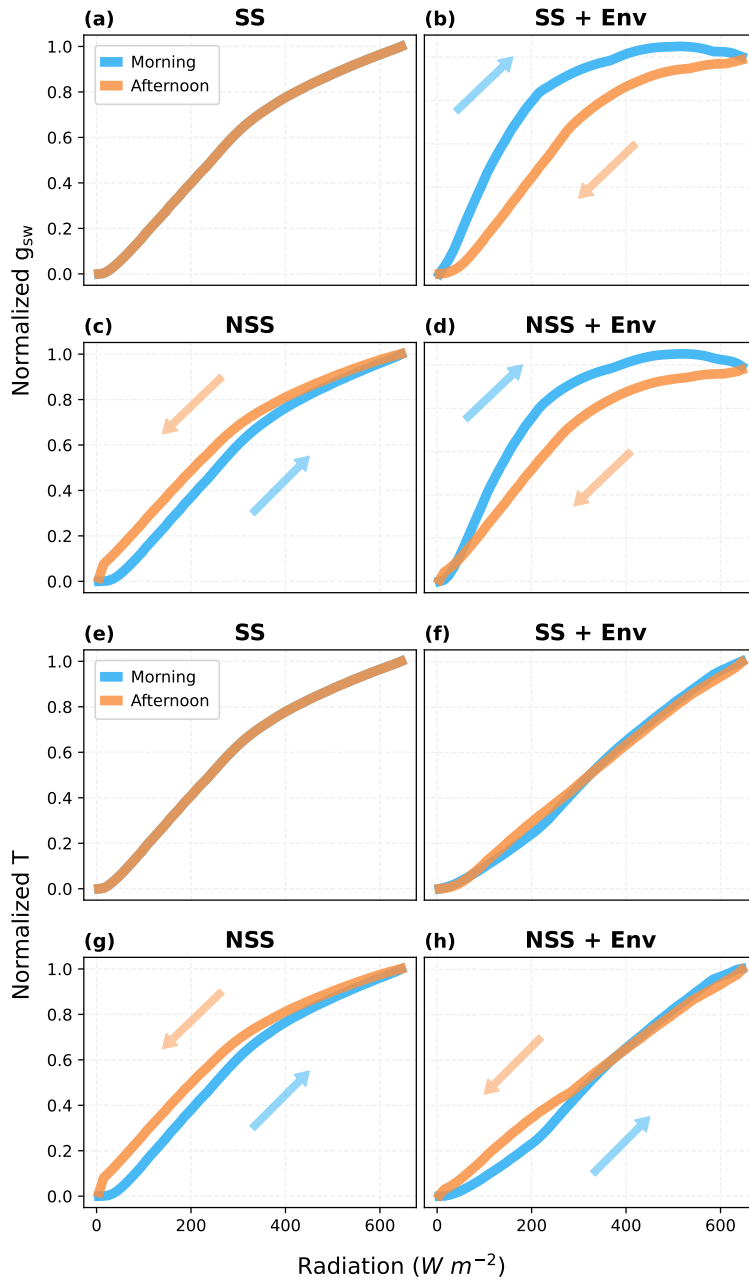


Figure S6: Hysteresis of the canopy-mean stomatal conductance (g_{sw}) and canopy transpiration rate (T) in response to radiation during an ideal clear-sky day, when $\tau_{op} = 300$ s, $\tau_{cl} = 900$ s. (a, e) SS model, (b, f) SS model with coupled diurnal variations of environmental conditions (Env, e.g. air temperature, VPD), (c, g) NSS model, (d, h) NSS model with Env. (a-d) normalized g_{sw} responses, (e-h) normalized T responses. In simulations without Env variations, except for the radiation, all the other environmental drivers were kept at the daytime means. g_{sw} and T is normalized with the values at noon (12:00). Arrows indicate the increasing and decreasing parts of the diurnal courses.

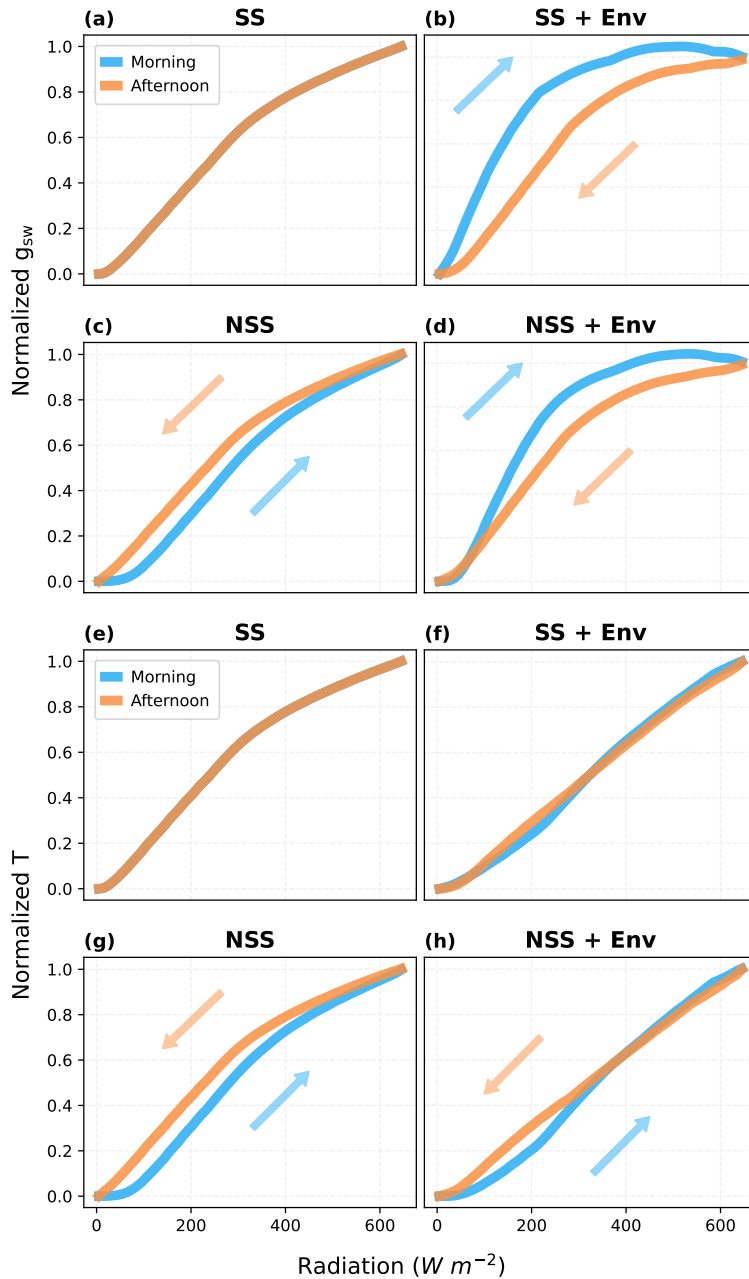


Figure S7: Hysteresis of the canopy-mean stomatal conductance (g_{sw}) and canopy transpiration rate (T) in response to radiation during an ideal clear-sky day, when $\tau_{op} = 900$ s, $\tau_{cl} = 300$ s. (a, e) SS model, (b, f) SS model with coupled diurnal variations of environmental conditions (Env, e.g. air temperature, VPD), (c, g) NSS model, (d, h) NSS model with Env. (a-d) normalized g_{sw} responses, (e-h) normalized T responses. In simulations without Env variations, except for the radiation, all the other environmental drivers were kept at the daytime means. g_{sw} and T is normalized with the values at noon (12:00). Arrows indicate the increasing and decreasing parts of the diurnal courses.

References

- Butler, E. E., Datta, A., Flores-Moreno, H., Chen, M., Wythers, K. R., Fazayeli, F., Banerjee, A., Atkin, O. K., Kattge, J., Amiaud, B., Blonder, B., Boenisch, G., Bond-Lamberty, B., Brown, K. A., Byun, C., Campetella, G., Cerabolini, B. E. L., Cornelissen, J. H. C., Craine, J. M., Craven, D., de Vries, F. T., Díaz, S., Domingues, T. F., Forey, E., González-Melo, A., Gross, N., Han, W., Hattingh, W. N., Hickler, T., Jansen, S., Kramer, K., Kraft, N. J. B., Kurokawa, H., Laughlin, D. C., Meir, P., Minden, V., Niinemets, Ü., Onoda, Y., Peñuelas, J., Read, Q., Sack, L., Schamp, B., Soudzilovskaia, N. A., Spasojevic, M. J., Sosinski, E., Thornton, P. E., Valladares, F., van Bodegom, P. M., Williams, M., Wirth, C., and Reich, P. B.: Mapping local and global variability in plant trait distributions, *Proceedings of the National Academy of Sciences*, 114, E10 937–E10 946, <https://doi.org/10.1073/pnas.1708984114>, publisher: Proceedings of the National Academy of Sciences, 2017.
- Croft, H., Chen, J. M., Wang, R., Mo, G., Luo, S., Luo, X., He, L., Gonsamo, A., Arabian, J., and Zhang, Y.: The global distribution of leaf chlorophyll content, *Remote Sensing of Environment*, 236, 111 479, iSBN: 0034-4257 Publisher: Elsevier, 2020.
- De Kauwe, M. G., Kala, J., Lin, Y.-S., Pitman, A. J., Medlyn, B. E., Duursma, R. A., Abramowitz, G., Wang, Y.-P., and Miralles, D. G.: A test of an optimal stomatal conductance scheme within the CABLE land surface model, *Geoscientific Model Development*, 8, 431–452, <https://doi.org/10.5194/gmd-8-431-2015>, publisher: Copernicus GmbH, 2015.
- Farquhar, G. D., von Caemmerer, S., and Berry, J. A.: A biochemical model of photosynthetic CO₂ assimilation in leaves of C₃ species, *Planta*, 149, 78–90, <https://doi.org/10.1007/BF00386231>, number: 1, 1980.
- He, L., Chen, J. M., Pisek, J., Schaaf, C. B., and Strahler, A. H.: Global clumping index map derived from the MODIS BRDF product, *Remote Sensing of Environment*, 119, 118–130, <https://doi.org/10.1016/j.rse.2011.12.008>, 2012.
- Hersbach, H., Bell, B., Berrisford, P., Biavati, G., Horányi, A., Muñoz Sabater, J., Nicolas, J., Peubey, C., Radu, R., Rozum, I., et al.: ERA5 hourly data on single levels from 1979 to present, Copernicus climate change service (c3s) climate data store (cds), 10, 2018.
- Luo, X., Keenan, T. F., Chen, J. M., Croft, H., Colin Prentice, I., Smith, N. G., Walker, A. P., Wang, H., Wang, R., Xu, C., and Zhang, Y.: Global variation in the fraction of leaf nitrogen allocated to photosynthesis, *Nature Communications*, 12, 4866, <https://doi.org/10.1038/s41467-021-25163-9>, number: 1 Publisher: Nature Publishing Group, 2021.
- van der Tol, C., Verhoef, W., Timmermans, J., Verhoef, A., and Su, Z.: An integrated model of soil-canopy spectral radiances, photosynthesis, fluorescence, temperature and energy balance, *Biogeosciences*, 6, 3109–3129, <https://doi.org/10.5194/bg-6-3109-2009>, publisher: Copernicus GmbH, 2009.
- Wang, Y., Braghieri, R. K., Longo, M., Norton, A. J., Köhler, P., Doughty, R., Yin, Y., Bloom, A. A., and Frankenberg, C.: Modeling Global Vegetation Gross Primary Productivity, Transpiration and Hyperspectral Canopy Radiative Transfer Simultaneously Using a Next Generation Land Surface Model—CliMA Land, *Journal of Advances in Modeling Earth Systems*, 15, e2021MS002 964, <https://doi.org/10.1029/2021MS002964>, eprint: <https://onlinelibrary.wiley.com/doi/pdf/10.1029/2021MS002964>, 2023.
- Yang, P., Verhoef, W., and van der Tol, C.: The mSCOPE model: A simple adaptation to the SCOPE model to describe reflectance, fluorescence and photosynthesis of vertically heterogeneous canopies, *Remote Sensing of Environment*, 201, 1–11, <https://doi.org/10.1016/j.rse.2017.08.029>, 2017.
- Yuan, H., Dai, Y., Xiao, Z., Ji, D., and Shangguan, W.: Reprocessing the MODIS Leaf Area Index products for land surface and climate modelling, *Remote Sensing of Environment*, 115, 1171–1187, <https://doi.org/10.1016/j.rse.2011.01.001>, 2011.